PCCP

Accepted Manuscript




ROYAL SOCIETY OF CHEMISTRY

www.rsc.org/pccp

PCCP

ARTICLE

# Mechanisms of AC losses in magnetic fluids based on substituted manganites

V.M. Kalita,[a] A.I. Tovstolytkin,[b†] S.M. Ryabchenko,[a] O.V. Yelenich,[c] S.O. Solopan,[c] A.G. Belous[c]

The ability to controllably tune the heating efficiency of magnetic nanoparticles in an AC magnetic field is highly desirable for their application as mediators of magnetic hyperthermia. Traditional approaches to understand and govern the behavior of hyperthermia mediators include a combination of quasistatic and high-frequency (~100 kHz) magnetic measurements with subsequent simulation of underlying processes. In this paper, we draw attention to frequently overlooked fact that for an ensemble of magnetic nanoparticles, there is no straightforward complementarity between the dynamic characteristics obtained under different experimental conditions, as well as between corresponding underlying processes. The paper analyzes mechanisms of AC losses in a fluid based on magnetic nanoparticles, with special emphasis on the domains of their validity, and shows that the mechanisms may become qualitatively different as experimental conditions change from magnetostatic to high-frequency ones. Further, the work highlights new important features which can result from the employment of the refined approaches to interpret experimental results obtained on magnetic fluids based on $La_{1-x}Sr_xMnO_3$ ($x$ = 0.22) nanoparticles. The gained knowledge provides necessary guidelines for tailoring the properties of magnetic nanoparticles to the needs of self-controlled magnetic hyperthermia.

Received 00th January 20xx,
Accepted 00th January 20xx

DOI: 10.1039/x0xx00000x

www.rsc.org/

## 1 Introduction

Nanosized particles of ferromagnetic (FM) materials are of considerable scientific interest due to the possibility of their use in engineering and medicine.[1-3] In the latter case, they can be used as contrast agents in magnetic resonance imaging, carriers of drugs, as well as mediators of hyperthermia (HT) of tumors.[3,4]

The concept of HT treatment is based on a higher heat sensitivity of tumor cells in comparison with healthy tissue. So, exposing the tissue to temperatures between 42 and 45 °C leads to destruction of the tumor cells and sparing of the healthy ones.[4,5] Magnetic HT is based on intravenous or intratumoral administration of magnetic nanoparticles (MNPs) into a tumor and subsequent exposure of the tumor to an alternating magnetic field (AMF).[5-8] With respect to the well-known medical restrictions on the upper limit of the product of the amplitude of the applied field $H_{max}$ and frequency $f$ ($H_{max}f$ has to be less than $5\times10^9$ $A\cdot m^{-1}\cdot s^{-1}$)[4,9,10] and the acceptable range of frequencies (the frequency $f$ has to be above 50 kHz to avoid neuromuscular electrostimulation and below 10 MHz to achieve a satisfactory depth of the penetration of AMF into the electrically conducting tissue[11,12]), a well-designed heating mediator with correctly adjusted magnetic properties is required.

Along with a need to satisfy a number of biomedical requirements (non-toxicity, biocompatibility with living organisms, etc.), the HT mediators have to demonstrate high heating efficiency when placed in AMF with corresponding parameters.[13] A quantitative measure of heating efficiency is specific loss power (SLP). The SLP, also referred to as specific absorption rate, represents the power dissipation per unit mass of MNPs subjected to AMF.

The results of the first researches into nanohyperthermia of tumors with the use of magnetite nanoparticles were described in Refs. [5,14-16]. The studies have shown that the use of $Fe_3O_4$ MNPs as HT mediators poses the risk of uncontrolled overheating of healthy tissues, due to nonuniform distribution of mediator particles throughout the tissue, variable AMF intensity and uneven dissipation of the evolving heat. Despite this, there is information on conducting the clinical trials of HT involving $Fe_3O_4$ MNPs coated with aminosilane as HT mediator.[17]

An important step towards the clinical application of magnetic HT will consist in achieving a reliable control of heating temperature (to exclude overheating) and increasing SLP value. To this end, research is under way to develop new materials.[18-22] It is known that magnetic materials provide more heating in the FM state (below Curie temperature, $T_C$) and, vice versa, considerably less heating in paramagnetic state (above $T_C$). Thus, the Curie temperature can act as a thermostatic switch, which maintains a constant desired temperature in the tumor region. In view of these facts, the MNPs of substituted lanthanum manganite $La_{1-x}Sr_xMnO_3$ ($x$ = 0.2 ÷ 0.4) are some of the best candidates for self-controlled HT applications because they not only have high SLP values at

[a] Institute of Physics of the NAS of Ukraine, 46 Nauky Ave., Kyiv 03028, Ukraine.
[b] Institute of Magnetism of the NAS of Ukraine, 36-b Vernadsky Ave., Kyiv 03142, Ukraine.
[c] V.I. Vernadskii Institute of General and Inorganic Chemistry of the NAS of Ukraine, 32/34 Palladin Ave., Kyiv 03142, Ukraine.
† Corresponding author: atov@imag.kiev.ua.

room temperature and above,[19,20,23-26] but also their Curie temperature can be easily adjusted between 315 and 350 K.[27-29]

Experiments on magnetic fluids based on substituted manganite MNPs have demonstrated high heating efficiency under AMF.[6,7,19,20,23-26] However, the mechanisms of AC losses in these materials remain to a large extent unclear. Along with traditionally considered processes of Neel-Brown relaxation and remagnetization based on Stoner-Wohlfarth model,[10,23,30,31,32,33] there are also ideas that due to significant magnetoresistance effects in the vicinity of the Curie point, eddy currents should be taken into account as a part of the heating mechanism.[34-36] It is also unclear how the relative contributions of the above mechanisms depend on MNP parameters and external factors (amplitude $H_{max}$ and frequency $f$ of AMF).

A traditional way to study the AC losses in MNPs is to extract necessary parameters of MNPs from magnetostatic measurements and use them to model remagnetization processes and calculate SLP values.[10-12,23-26,30] It should be noted, however, that some parameters, which describe magnetic behavior of MNPs, are not intrinsic; they depend on external factors, namely, on AMF frequency and amplitude.[10,31,32,37] This means that not only the SLP values calculated with the use of magnetostatic parameters could be incorrect, but also the mechanisms of AC losses could become different as measurement conditions change from magnetostatic to high-frequency ones.

The aim of this work is to analyze the mechanisms of heating efficiency of magnetic fluids based on MNPs, estimate the SLP values related to each of the mechanisms, determine the ranges of external parameters for which the SLP estimations are valid, and employ these calculations to interpret experimental results obtained on magnetic fluids based on $La_{1-x}Sr_xMnO_3$ ($x$ = 0.22) MNPs.

## 2 Mechanisms of AC losses

### 2.1. General considerations

If magnetic fluid based on single domain ferromagnetic nanoparticles is subjected to AMF action, a part of the field energy is dissipated by the nanoparticles and transformed into heat. For magnetic HT, low-concentrated suspensions of MNPs in dielectric fluids are usually used.[4-6] In this case, inter-particle interaction is assumed to be negligible and the energy dissipation can be described as a sum of processes occurring in separate particles.

For a comprehensive analysis of the mechanisms of AC losses, one should consider the losses related to:

(A) excitation of eddy currents (EC-losses);

(B) remagnetization of a particle;

(C) rotation, induced by AMF, of a particle as a whole; usually termed Brown relaxation (BR-losses).

The processes underlying various types of losses are schematically shown in Fig. 1.

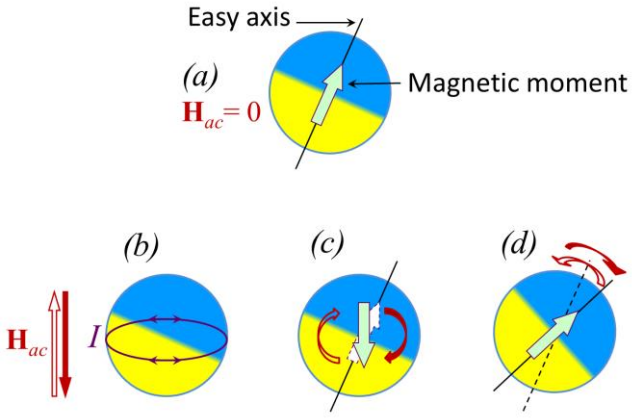


**Fig. 1** Illustration of the processes underlying various types of AC losses in a MNP subjected to the action of magnetic field $\mathbf{H}_{ac}$: (*a*) initial state of a MNP; (*b*) excitation of eddy currents (EC-losses); (*c*) losses related to particle remagnetization; (*d*) particle rotation induced by magnetic field (BR-losses).

Below, the calculations will be carried out for the power losses per second, normalized to the unit of volume of a nanoparticle. This quantity will be denoted as $P$. With the use of the MNP density, $\rho^{MNP}$, one can easily recalculate obtained quantity into SLP:

$$SLP = P / \rho^{MNP}. \qquad (2.1)$$

### 2.2. Description of the losses

**2.2(A). EC-losses.** The losses related to the first mechanism (EC-losses) become relevant when material subjected to AMF action has high electric conductivity. The conductivity σ of the materials, which are considered as pretenders for magnetic HT mediators, can be quite high. So, for the spinel ferrites σ can reach $10^5$ $\Omega^{-1}m^{-1}$, [38,39] for substituted manganites – $10^6$ $\Omega^{-1}m^{-1}$. [27] Some researchers discuss the possibility of using metallic MNPs ($\sigma \geq 10^8$ $\Omega^{-1}m^{-1}$) covered with an inert (biocompatible) shell in magnetic HT.[10,24] For this reason, the answer to the question whether or not one can neglect EC-losses in the cases under consideration is not trivial.

For a spherical particle, which has radius $R$, conductivity σ and is under the action of AMF with a frequency $f$, an average value of EC-losses calculated per unit of a particle volume is described by a formula:[40]

$$P_{EC} = \frac{\sigma}{5}\pi^2 f^2 B_{max}^2 R^2 = \frac{\sigma}{5}\pi^2 f^2 \mu_0^2 (H_{max} + M_{max})^2 R^2, \qquad (2.2)$$

where $B_{max}$, $H_{max}$ and $M_{max}$ are the amplitudes of magnetic induction, magnetic field and particle magnetization, respectively, $\mu_0$ – the magnetic constant ($\mu_0 = 4\pi\cdot10^{-7}$ H/m). For the case of weak magnetic fields, namely, when magnetization $M$ is a linear function of external magnetic field $H$ ($M = \chi H$), expression (2.2) is transformed into the following:

$$P_{EC} = \frac{\sigma}{5}\pi^2 f^2 \mu_0^2 (1+\chi)^2 H_{max}^2 R^2 = \frac{\sigma}{5}\pi^2 f^2 \mu_0^2 \mu^2 H_{max}^2 R^2. \qquad (2.3)$$

Here, $\chi$ is the magnetic susceptibility of the ensemble of particles and $\mu$ is the relative magnetic permeability ($\mu = 1 + \chi$).

In this regime, $P_{EC}$ displays quadratic dependence on both AMF amplitude $H_{max}$ and frequency $f$.

**2.2(B). Remagnetization losses.** The losses associated with MNP remagnetization depend on relation between the characteristic parameters of nanoparticles (saturation magnetization $M_s$, effective magnetic anisotropy constant $K_{eff}$, coercivity $H_c$, nanoparticle volume $V$, relaxation time of a nanoparticle system $\tau$) and external parameters (amplitude $H_{max}$ and frequency $f$ of external magnetic field, temperature $T$).

The behavior of single domain MNPs depends on the energy balance between anisotropy ($\varepsilon_a = K_{eff} \cdot V$) and thermal fluctuation ($\varepsilon_T \approx k_B \cdot T$) contributions (here, $k_B$ is the Boltzmann constant). In the limit $\varepsilon_T >> \varepsilon_a$, the magnetic moment of a particle can be considered as freely fluctuating. This results in the phenomenon of superparamagnetism, where the ensemble of particles behaves like a paramagnet consisting of particles with very large magnetic moments. In the opposite limit, when $\varepsilon_T << \varepsilon_a$, the particle magnetic moment is blocked on a time scale given by the experiment and lies parallel or antiparallel to the easy magnetization axis. The transition to the latter state occurs at the so-called blocking temperature $T_b$, below which the particle moments appear frozen on the time scale of the measurement $\tau_m$. The $T_b$ value depends on the measurements duration and can be determined from the temperature dependences of magnetization: the zero-field-cooled (ZFC) magnetization $M_{zfc}$ measured in a weak magnetic field achieves a maximum at $T_b$.[37] The ZFC magnetization curve is usually measured in quasistatic measurements with increasing temperature in a weak magnetic field after cooling the specimen in absence of magnetic field down to $T << T_b$. The measurement duration in such case is of order of hundreds of seconds.

**2.2(B1). Neel relaxation (NR-losses).** Consider in more detail the processes occurring within the transitional region from equilibrium superparamagnetism to the blocked state. As temperature is lowered, the energy of thermal fluctuations decreases and eventually becomes comparable to the anisotropy energy. Experiments show that in majority of cases the effective magnetic anisotropy of nanoparticles is uniaxial, independent of the symmetry of crystalline lattice and contributions from shape, strain and surface anisotropies.[26,31,37] Thus, as a function of angle $\theta$ between the directions of MNP magnetic moment and easy magnetization axis, the MNP free energy achieves a minimum when $\theta$ equals either 0 or $\pi$ (Fig. 2(*a*,*b*)). These two states are divided by an energy barrier whose height is $\varepsilon_a$. Application of external magnetic field decreases the energy for one of the states and increases for another one (Fig. 2(*c*)). In this case, the probability of the population of the state with lower energy becomes higher, but the processes of the state repopulation are not straightforward and do not occur instantaneously.

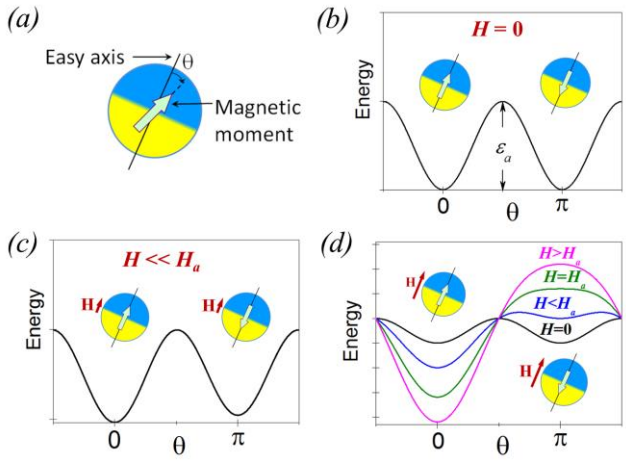


**Fig. 2** Schematic pictures of a single domain particle with uniaxial anisotropy (*a*) and its energy landscape in different magnetic fields: $H = 0$ (*b*), $H << H_a$ (*c*), $H$ = var (*d*). $H_a$ is the effective anisotropy field of the particle, $\varepsilon_a$ is the energy barrier hindering free rotation of magnetization and $\theta$ is the angle between the MNP magnetic moment and easy axis.

If inequality $\varepsilon_T \geq \varepsilon_a$ keeps valid, the particle magnetic moments still overcome the threshold by thermal energy, but encounter a hindered rotation due to the finite height of the barrier. The system gets into the equilibrium during a characteristic time $\tau$ which is strongly temperature-dependent. For times much longer than $\tau$, the system has enough time to reach equilibrium and the probability of finding the magnetic moment in one of the two minima is independent of the initial state (non-hysteretic non-coercive behavior). By contrary, for times much shorter than $\tau$, the magnetic moment remains in its initial minimum and, thus, its behavior depends on thermal and magnetic prehystory (hysteretic coercive behavior). As a result of all the above processes, the resulting behavior of the system is determined by the interplay of a few factors: (1) the value of magnetic field $H_{max}$ (how strongly magnetic field modifies the energy barrier); (2) temperature $T$ (how fast or slow are thermally activated processes facilitating establishment of equilibrium); (3) time scale of the measurement $\tau_m$ (a relation between $\tau_m$ and $\tau$ determines whether or not the system has enough time to get into the equilibrium during the time of measurement).

If thermally activated fluctuations of the magnetic moment direction are fast compared to the measurement duration ($\tau < \tau_m$), one can say about the Neel relaxation (also termed Neel-Arrhenius or Neel-Brown relaxation). To describe the remagnetization processes in this regime, two cases should be distinguished.

If *magnetic field is so weak* that it scarcely affects the height of the energy barrier ($H_{max} << H_a$, where $H_a$ is the anisotropy field: $H_a = 2K_{eff}/M_s$, with $M_s$ being saturation magnetization of the particle[37]), the behavior of the ensemble of MNPs can be described by a linear response theory (LRT) with relaxation time taken in Neel-Brown form:[31]

$$\tau = \tau_0 \cdot \exp(K_{eff} V / k_B T), \qquad (2.4)$$

where $\tau_0 \sim 10^{-9}$ s is the inverse attempt frequency.[4,31,37]

The fact that τ is finite means that remagnetization of MNP ensemble does not occur instantaneously and, thus, the average magnetization tracks the magnetic field with delay. Time dependence of the magnetization of MNP ensemble ( $\tilde{M}$ ) is described by a relaxation equation:

$$\frac{d\tilde{M}(t)}{dt} = \frac{1}{\tau}(\tilde{M}_0(H(t)) - \tilde{M}(t)), \qquad (2.5)$$

where $\tilde{M}$ and $\tilde{M}_0$ are respectively the instant and equilibrium values of the magnetization in the field with strength *H*.

For the case of harmonic magnetic field with angular frequency $\omega = 2\pi f$ a solution of equation (2.5) allows calculating magnetic susceptibility:

$$\chi \equiv \frac{\tilde{M}}{H} = \frac{\chi_0}{1+i\omega\tau} = \frac{\chi_0}{1+(2\pi f\tau)^2} - \frac{i2\pi f\tau\chi_0}{1+(2\pi f\tau)^2} = \chi' - i\chi'', \qquad (2.6)$$

where $\chi_0$ is the equilibrium magnetic susceptibility $\left(\chi_0 = d\tilde{M}_0 / dH\big|_{H\to 0}\right)$. The value of $\chi_0$ can be determined from quasistatic measurements, i.e. from the measurements which are so slow that during the time of measurements the magnetization has enough time to reach the equilibrium state. Susceptibility (2.6) can be considered as a physical quantity which characterizes the response of the system, whose state is close to the equilibrium, to the action of weak alternating magnetic field.

Writing expression for magnetic susceptibility in form (2.6) implies that the response of the magnetic system to the change of magnetic field is linear. That is why the theory which employs this expression is called linear response theory. The use of this expression is only correct when the deviation of instant magnetization from equilibrium value is small:

$$\left|\tilde{M}_0 - \tilde{M}\right| << \tilde{M}_0 . \qquad (2.7)$$

Magnetic susceptibility (2.6) contains real ("elastic") and imaginary components. Thermal losses result from the latter. Keeping in mind the approximations described above, one can write the expression for the specific power dissipated by an ensemble of MNPs:

$$P_{NR} = f\mu_0 \int_0^{1/f} \tilde{M}dH = f\pi\mu_0\chi'' H_{\max}^2 = \frac{2\mu_0\pi^2 f^2\tau}{1+(2\pi f\tau)^2}\chi_0 H_{\max}^2 . \qquad (2.8)$$

It is seen that $P_{NR}$ displays a quadratic dependence on AMF amplitude $H_{max}$. As a function of frequency, it is quadratic at low values of *f* ($2\pi f\tau << 1$), deviates from quadratic law as *f* increases and tends to a saturation at high frequencies ($2\pi f\tau >> 1$), where the saturated value reads:

$$P_{NR}^{f\to\infty} = \frac{\mu_0\chi_0 H_{\max}^2}{2\tau} . \qquad (2.9)$$

Heating efficiency under such conditions ($2\pi f\tau >> 1$) does not depend on frequency.

For the case where *magnetic field is not weak, i. e. when it affects the height of energy barrier* ($H_{max}$ is comparable to $H_a$), only numerical simulation is correct for the description of the behavior of MNPs. The approaches which describe the algorithms of the numerical calculations have been presented in Refs. [4,7,10,30,31].

It is noteworthy that magnetic fields which are used in hyperthermia ($\mu_0 H_{max}$ ~ 10 mT) cannot be considered as weak. As a rule, they strongly affect the height of energy barrier. For this reason, the use of formulae (2.6) – (2.9) for the description of the Neel mechanism of relaxation within the region of temperatures comparable or higher than room temperature is often incorrect.

The question as to whether LRT with the use of the relaxation time in the Neel-Brown form can be employed to calculate the power of losses in those MNPs which are promising candidates for magnetic HT mediators was discussed in Refs. [4,11,31]. It was concluded that LRT has a very restricted domain of validity. First, the use of this approach is correct for any value of magnetic field only for small MNPs, for which the inequality $K_{eff}V << k_BT$ is valid in the vicinity of room temperature. It is noteworthy, however, that the MNPs in this range are useless for magnetic HT due to negligible $P_{NR}$ values ($\tau$ ~ 0 in expression (2.8)). Second, LRT allows one to calculate the AC-losses for larger nanoparticles, but only at relatively small fields ($H_{max} << H_a$). Since $\mu_0 H_{max}$ in HT is of the order of 10 mT, LRT can be valid only in the case of strongly anisotropic nanoparticles ($K_{eff} > 10^5$ J/m$^3$). However, one should keep in mind that the increase in the MNP anisotropy results in the increase of blocking temperature and when $T_b$ value crosses room temperature, the NR-approach again becomes invalid for the description of power losses at room temperature and above. In addition, if such MNPs are able to freely rotate in magnetic fluid, a considerable part of power can be spent on particle rotation (BR-losses).

**2.2(B2). Remagnetization based on Stoner-Wohlfarth model (SW-losses).** If thermally activated fluctuations of the magnetic moment direction are not fast in comparison with the measurement duration ($\tau > \tau_m$), the system is in the blocked state and the dependence of power losses on magnetic field is of threshold character.

For the case of *weak magnetic fields* ($H_{max} << H_a$), the reaction of the system to external magnetic field will be very weak, remagnetization practically won't occur (only minor hysteresis loop will be observed), and, thus, the power of dissipation will be negligible. If *amplitude of magnetic field equals or exceeds anisotropy field*, the shape and area of hysteresis loop will approach, but won't exceed a theoretical limit which is described by the Stoner-Wohlfarth model.[21]

Stoner and Wohlfarth considered non-interacting particles with uniaxial anisotropy, in which the spins are parallel and rotate coherently. The original Stoner-Wohlfarth model does not take into account any thermal activation, and, thus, it is relevant at *T* = 0. As a consequence of neglecting thermal activation, the magnetization can only stay along one of the two equilibrium positions (parallel or antiparallel to the easy magnetization axis). The switch of the magnetization from the metastable state to the equilibrium position can only occur when the energy barrier is fully removed by magnetic field



 

(Fig. 2(*d*)). To take into account thermal activation and perturbative time scale, an effective $H_c$ can be considered to vary with the frequency of AC magnetic field (due to the dependence of $\tau/\tau_m$ ratio on remagnetization frequency) and temperature.

If an ensemble of MNPs is put into an AMF, the amount of heat dissipated in MNPs during one cycle of the magnetic field is equal to the area of hysteresis loop *S*. The dissipated energy per second per unit volume of MNPs is then given by:

$$P_{SW} = Sf \ . \tag{2.10}$$

For a MNP in a blocked state and with its easy axis aligned along the magnetic field direction, the hysteresis loop is a rectangle with temperature-dependent $H_c$. At low temperatures ($T \to 0$), the temperature activated repopulation of energy minima is suppressed, and remagnetization can only occur when the energy barrier is fully removed by magnetic field. This occurs when $H_{\max}$ reaches anisotropy field $H_a$ (see Fig. 2(*d*)). Thus, for the Stoner-Wohlfarth model $H_c \to H_a$ as $T \to 0$. For an optimal case where $H_{\max} = H_c$:

$$P_{SW} = 4\mu_0 H_{\max} M_s f \ . \tag{2.11}$$

To estimate $P_{SW}$ in all other cases, it is convenient to use formula

$$P_{SW} = 4\alpha\mu_0 H_{\max} M_s f \ , \tag{2.12}$$

where $\alpha$ is a dimensionless parameter which equals the ratio between the areas of actual hysteresis loop and ideal rectangle loop, with the latter having $\alpha = 1$. For the ensemble of MNPs with randomly oriented anisotropy axes and optimally chosen relation between $H_c$ and $H_{\max}$ ($H_c = 0.81H_{\max}$), $\alpha = 0.39$.[10,31] When $H_{\max}$ is less than a field at which magnetization saturation occurs, $\alpha$ is a function of $H_{\max}$.

As a result, the upper limit of $P_{SW}$ for the ensemble of MNPs with randomly oriented anisotropy axes is:

$$P_{SW}^{\text{limit}} = 4 \cdot 0.39 \cdot \mu_0 H_{\max} M_s f \ . \tag{2.13}$$

The values of $\alpha$ observed in experiment do not exceed 0.3. [10,31]

**2.2(C). BR-losses.** In fluid suspensions, the relatively high anisotropy barrier may be overcome by rotation of the whole particle under the influence of AMF. In this case, frictional losses due to viscosity $\eta$ of the carrier liquid arise. The resulting relaxation time is given by:[4]

$$\tau_B = \frac{4\pi\eta R_h^3}{k_B T} \ , \tag{2.14}$$

where $R_h$ is the hydrodynamically effective radius, which may differ from the geometrical one.[4,5,13] The process is commonly termed Brown relaxation.

In a general case, both processes, Brown relaxation and particle remagnetization, are present, but the faster one is dominant, and an effective relaxation time may be defined by

$$\frac{1}{\tau_{eff}} = \frac{1}{\tau} + \frac{1}{\tau_B} \ . \tag{2.15}$$

A traditional way to account for both kinds of losses is to use LRT (see formula (2.8)) with effective relaxation time $\tau_{eff}$ instead of $\tau$.[4,10,31] What concerns the domain of validity of such approach, it is pertinent to make two remarks. (1) As was mentioned above, the use of LRT is only correct when the deviation of instant magnetization from equilibrium value is small. (2) If magnetic field becomes high enough to affect the height of energy barrier, the Brown relaxation weakens and gets completely suppressed as $H_{\max}$ exceeds anisotropy field $H_a$.

### 2.3. Effects of experimental conditions on AC-losses

**2.3.1. Low-frequency and high-frequency measurements.** In the remainder of this paper, the measurements in magnetic fields whose frequency *f* is of the order of hundreds of kHz will be termed high-frequency (HF) measurements, while measurements with *f* less than hundreds of Hz, including quasistatic ones, will be termed low-frequency (LF) measurements.

A usual way to model remagnetization processes and calculate *SLP* values is to use the MNP parameters extracted from LF measurements.[10-12,23-26,30,41] It should be noted, however, that such parameters as blocking temperature $T_b$ and coercivity $H_c$ are frequency-dependent. This means that not only *SLP* values calculated with the use of magnetostatic parameters could be incorrect, but also the mechanisms of AC losses could become different as measurement conditions change from magnetostatic to HF ones.

It was noted above that blocking temperature $T_b$ is the temperature at which a condition

$$\tau_m = \tau\big|_{T=T_B} \tag{2.16}$$

is satisfied. At this temperature the rate of thermally activated processes becomes insufficient to get the system into equilibrium, and MNP magnetic moment remains blocked in a metastable state. Formulae (2.4) and (2.16) make it possible to estimate the dependence of blocking temperature on measurement time. Assuming that a time scale of measurements is $1/f$, $T_b$ can be roughly estimated as

$$T_b \approx K_{eff} V \Big/ \left( k_B \ln(\frac{1}{f\tau_0}) \right). \tag{2.17}$$

If MNP magnetic parameters, in particular $K_{eff}$, were temperature independent, the change of the AMF frequency from ~0.01 Hz (magnetostatic measurements) to ~$10^5$ Hz (the frequencies at which usually HT treatment is carried out) would result in the increase of $T_b$ by (2 ÷ 3) times. Thus, for the case where the $T_b^{lf}$ value exceeds ~150 K, the $T_b^{hf}$ value can exceed room temperature. This means that the mechanism responsible for AC losses in the vicinity of room temperature will be SW-mechanism, rather than NR-one, as follows from LF measurements.

Fig. 3 illustrates $M_{zfc}^{lf}(T)$ and $M_{zfc}^{hf}(T)$ dependences obtained from LF and HF measurements, respectively. For each of these curves, magnetization reaches a maximum at temperature which equals the blocking temperature. Since $T_b^{lf} << T_b^{hf}$, the temperature region within which SW-mechanism is responsible for the losses is by far wider in the latter case (HF measurements), than in the former one (LF measurements).

The scheme in Fig. 3 is given under the assumption that $T_b^{hf} << T_C$. For the case, where $T_b^{hf}$ is close to $T_C$, the relation between $T_b^{lf}$ and $T_b^{hf}$ will qualitatively be the same, but quantitative difference between them will change. Naturally, $T_b$ cannot exceed $T_C$.

**2.3.2. Dependence on magnetic field.** Magnetic field affects the height of energy barrier and, thus, the value of blocking temperature. Formula (2.17) determines the $T_b$ value for an ideal case of zero magnetic field. With the increase in AMF strength $H$, blocking temperature decreases according to the power law:

$$T_b(H) = T_b(0)\left(1 - \frac{H}{H_c}\right)^k, \qquad (2.18)$$

where $k$ = 2 for weak fields and 2/3 for strong ones[37] (Fig. 4).

## 3 Experiment

### 3.1. Justification of the choice of MNP chemical composition and synthesis method

Magnetic state of $La_{1-x}Sr_xMnO_3$ manganites strongly depends on strontium content $x$.[26-28] Bulk samples with $0.15 \le x \le 0.60$ are ferromagnetic.[27,28] Curie temperature $T_C$ displays a maximum at $x$ = 0.33 ($T_{Cmax} \cong 370$ K) and is reduced as $x$ deviates from 0.33.

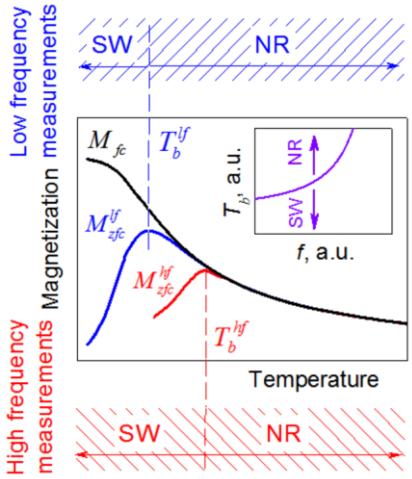


**Fig. 3** Illustration of the behavior of magnetization resulted from LF and HF measurements. Inset presents frequency dependence of blocking temperature $T_b$. $M_{fc}$ – field-cooled magnetization, $M_{zfc}^{lf}$ and $M_{zfc}^{hf}$ – the zero-field-cooled magnetization values resulted from LF and HF measurements, respectively. $T_b^{lf}$ and $T_b^{hf}$ – the values of blocking temperatures resulted from LF and HF measurements, respectively. Top and bottom diagrams schematically illustrate temperature regions, where either SW-, or NR-mechanism of losses dominates for LF and HF cases, respectively.

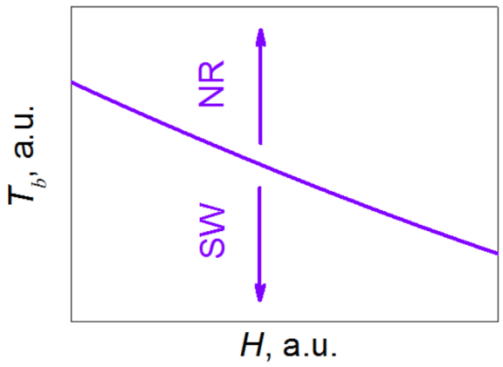


**Fig. 4** Illustration of the dependence of blocking temperature $T_b$ on magnetic field strength $H$. The arrows indicate temperature regions where either SW-, or NR-mechanism of losses dominates.

So, the decrease of $x$ from 0.33 to 0.20 leads to $T_C$ reduction from 370 to 309 K.[27] The same trend keeps for $La_{1-x}Sr_xMnO_3$ nanoparticles.[25,42] Since the development of self-controlled heating mediators for HT requires MNPs with $T_C$ close to 320 K, in this work the $La_{1-x}Sr_xMnO_3$ MNPs with $x$ = 0.22 were chosen for investigations.

To date, researchers have employed various methods to synthesize MNPs: sol-gel method, coprecipitation from aqueous solutions, microwave refluxing technique, and a number of others.[1,5,10,11,21,24,25,43,44] However, the use of such methods, as a rule, does not allow one to obtain weakly agglomerated nanoparticles; in most cases this is hindered by a formation of interparticle bridges.[7,24] At the same time, as shown in Refs. [7,30,41,43], the use of the methods based on synthesis from nonaqueous solutions or precipitation from microemulsions makes it possible to prevent MNP agglomeration, due to the isolation of nanoparticles from each other in the process of synthesis. For this reason, in this work a method of precipitation from microemulsions was chosen to obtain the MNPs of substituted manganites.

### 3.2. Experimental details

The synthesis of $La_{1-x}Sr_xMnO_3$ ($x$ = 0.22) (hereafter – LSMO) MNPs was carried out by the method of precipitation from microemulsions.[7,44] Water-soluble $La(NO_3)_3$, $Sr(NO_3)_2$, $Mn(NO_3)_2$ metal salts and 25% ammonia solution were used as starting reagents and precipitant, respectively. As a surfactant, the polyoxyethylene octyl phenyl ether (Triton X-100) was employed. All chemicals were purchased from Sigma–Aldrich. When creating microemulsions, the cyclohexane and butyl alcohol were chosen as the oil phase and co-surfactant. Bidistilled water was used as a dispersion medium and solvent. LSMO MNPs were synthesized by mixing two microemulsions: the first one contained salts of lanthanum, strontium and manganese, the second - precipitant.

To prepare the microemulsions, the ratio of components was adjusted in accordance with the procedures described in Refs. [45,46]. The components of the microemulsion were mixed in the following weight ratio: metal salt - 11%, surfactant - 11%, cyclohexane - 65%, butanol - 13%. Ammonia microemulsion was slowly added dropwise into microemulsion



 

of metal salts with interval of 4-5 s per one drop accompanied by constant stirring. The synthesis was carried out at 100 °C for 1 hour with vigorous stirring. The resulting product was separated by centrifugation, washed with methanol, and subsequently dried under air. The resultant amorphous nanoparticles were calcined at temperatures in the range of 200–800°C (in ambient air) to obtain the single phase product.

Nanoparticles were characterized by a DRON-4 X-ray diffractometer for phase and structure identification. The morphology and particle size were studied with the use of transmission electron microscopy (JEM-1230). Magnetic measurements were performed in the (10÷390) K temperature range using a LDJ-9500 vibrating sample magnetometer. For the calorimetric determination of specific loss power which is released on the exposure of an ensemble of the particles to AMF, the ferrofluids based on synthesized MNPs (50 mg/mL) were prepared using 0.1 % aqueous agarose solutions[6,7] and placed in the middle of a coil (5 turns, diameter 3 cm), which induced AMF with amplitude $\mu_0 H_{max}$ up to 12.5 mT with different frequencies up to 400 kHz. The details of the *SLP* measurements were described in Refs. [7,30,47].

### 3.3. Experimental results

**3.3.1. X-ray diffraction and TEM data.** XRD experiments have shown that LSMO powder obtained at 100 °C is amorphous (Fig. 5). Chemical analysis of the solution which remained after the powder was washed off showed that there occurred complete precipitation of chemical elements with maintaining stoichiometry according to the preset nominal composition.

To obtain crystalline structure, the powder was subjected to additional heat treatment at temperatures from 200 to 800 °C. It was revealed that crystalline phase started forming after heat treatment at 600 °C. Further experiments showed that heat treatment at higher temperatures lead to the change in both linewidths and intensities of the X-ray diffraction peaks, which implied that the powder still contained the remains of amorphous phase. A rise in temperature up to 800 °C resulted in complete crystallization of particles.

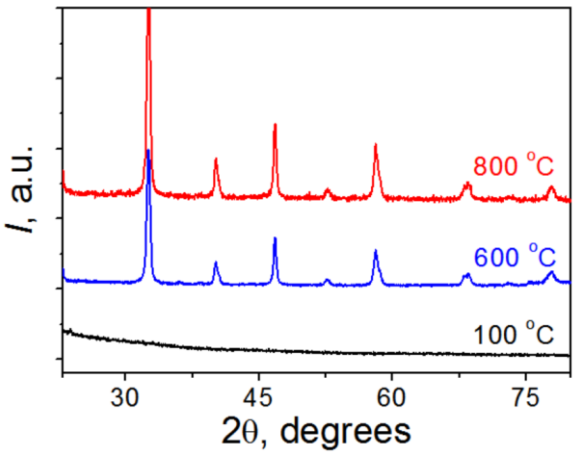


**Fig. 5** X-ray diffractograms for LSMO MNPs subjected to heat treatment at different temperatures.

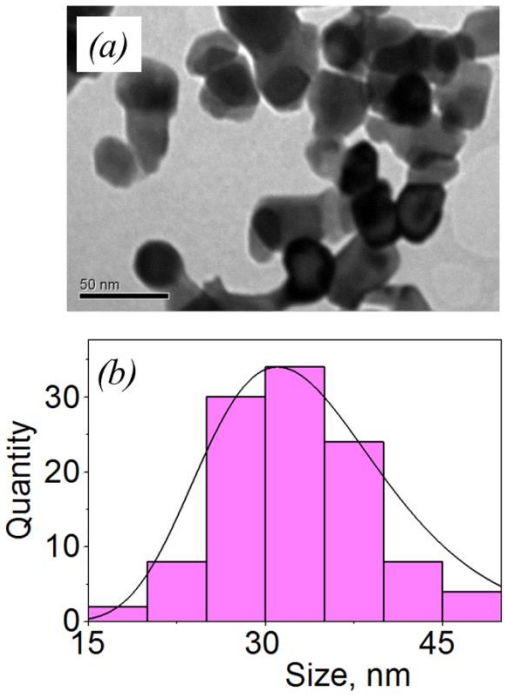


**Fig. 6** Microphotograph of LSMO MNPs (*a*) and diagram of their distribution in size (*b*).

As follows from electron microscopy studies, the particles obtained after heat treatment at 600 – 800 °C are weakly agglomerated. Average size of MNPs depends on temperature and/or duration of heat treatment.

Fig. 6(a) shows a typical microphotograph of LSMO MNPs which were studied in this work. The distribution of particles in sizes was calculated according to the method described in Ref. [48]. It was found that more than 80 % of MNPs have sizes in the range from 25 to 40 nm; the average MNP size is near 32 nm (Fig. 6(b)).

**3.3.2. Quasistatic magnetic properties.** Fig. 7 shows temperature dependences of mass magnetizations $M^m_{fc}$ and $M^m_{zfc}$, obtained in magnetic field $\mu_0 H$ = 2 mT.

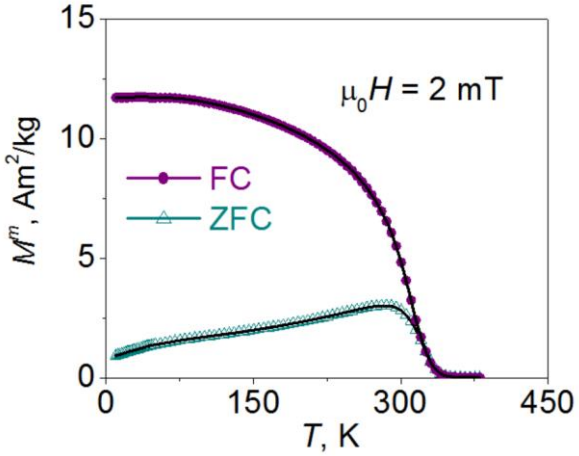


**Fig. 7** Temperature dependences of mass magnetizations $M^m_{fc}$ and $M^m_{zfc}$ for LSMO MNPs.

The $M^m_{fc}(T)$ and $M^m_{zfc}(T)$ curves coincide at temperatures higher than 320 K, but diverge in the low-temperature region. $M^m_{fc}$ is a declining function of temperature, while $M^m_{zfc}(T)$ is a curve with a maximum. The quasistatic (i.e. low-frequency, with $10^{-4} < f < 10^{-2}$ s$^{-1}$) blocking temperature, defined as a temperature at which $M^m_{zfc}(T)$ achieves a maximum, is $T_b^{lf}$ = 285 K.

Magnetization loops $M^m(H)$ obtained at $T$ = 10 and 295 K are presented in Fig. 8. Both curves display a tendency to saturation in strong fields ($\mu_0 H$ > 300 mT). The values of saturation magnetization, defined as magnetization in a field of 1 T, are: $M_s^m|_{T=10\text{ K}} \approx 81$ A·m$^2$/kg and $M_s^m|_{T=295\text{ K}} \approx 47$ A·m$^2$/kg. The $M^m$ vs $H$ curves are characterized by coercivities $\mu_0 H_c \approx 22.7$ and 1.2 mT at $T$ = 10 and 295 K, respectively (see inset of Fig. 8).

**3.3.3. Heating characteristics.** To obtain the AC magnetic heating characteristics of the synthesized MNPs, the time dependence of heat generation was studied under AC magnetic field with fixed amplitude $H_{max}$ and frequency $f$ of AMF.[3,16] Representative plots of magnetic fluid temperature versus residence time in external AMF ($f$ = 300 kHz, $\mu_0 H_{max}$ = (2 ÷ 12.5) mT) for the fluids based on synthesized MNPs are shown in Fig. 9. Each symbol in the figure is the result of averaging the data over 3 measurements on different portions of synthesized MNPs (the reproducibility of experimental results is no worse than 5 %).

One should note two characteristic features of the behavior of the AC magnetic heating characteristics. (1) For the fields with $\mu_0 H_{max}$ less than ~5 mT, the temperature of magnetic fluid remains almost unchangeable. (2) For the fields with $\mu_0 H_{max}$ exceeding ~10 mT, the temperature of magnetic fluid goes to a saturation value $T_s \approx 62$ °C.

The latter fact confirms the initial idea that the heating efficiency becomes strongly weakened when MNPs undergo the transition into paramagnetic state. It also means, however, that further experiments should be carried out to shift $T_s$ value to the region suitable for HT.

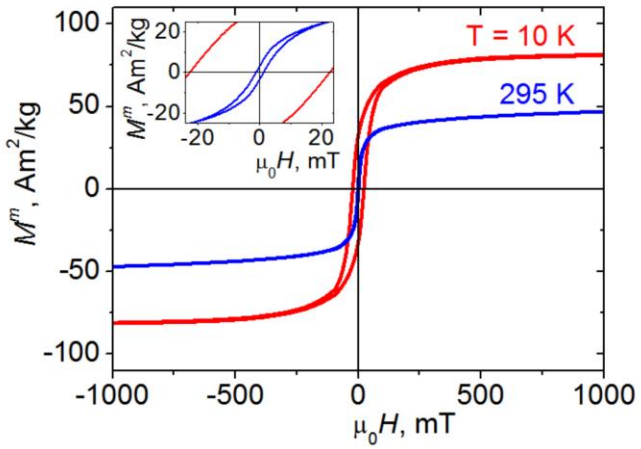


**Fig. 8** Magnetization loops $M^m(H)$ at $T$ = 10 and 295 K. Inset shows the same dependences in the region of weak fields.

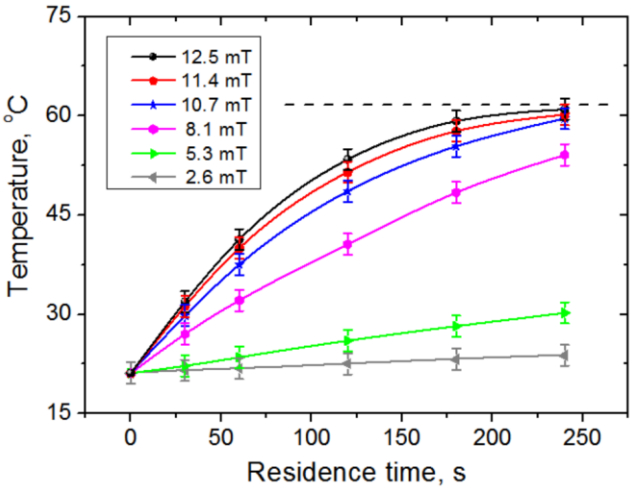


**Fig. 9** Representative plots of magnetic fluid temperature versus residence time in external AMF ($f$ = 300 kHz, $\mu_0 H_{max}$ = (2 ÷ 12.5) mT) for the fluids based on synthesized MNPs.

The initial slope of each curve plotted in Fig. 9 provides information about specific loss power.[6,21] The *SLP* values, which depend on the parameters of applied AC field, were calculated for a range of magnetic field amplitudes $\mu_0 H_{max}$ (from 2 to 12.5 mT) and frequencies ($f$ = 100, 200, 300 and 400 kHz). The details of the *SLP* calculation are described in Refs. [7,30,47].

Fig. 10 shows *SLP* vs $H_{max}$ dependence obtained at $f$ = 300 kHz. *SLP* is negligibly small at weak magnetic fields ($\mu_0 H_{max}$ < 5 mT), rapidly rises in the region from ~5 to ~10 mT, and then displays a tendency to saturation. In the region from 6 to 9 mT the *SLP*($H_{max}$) dependence is almost linear.

Inset of Fig. 10 presents the *SLP* vs $f$ dependence obtained in a field of $\mu_0 H_{max}$ = 10 mT. This dependence is almost linear, which implies that the losses per one remagnetization cycle are almost independent of frequency and equal to:

$$\frac{SLP}{f}\Big|_{\mu_0 H_{max}=10\text{ mT}} = 0.082\text{ J/kg}\,. \qquad (3.1)$$

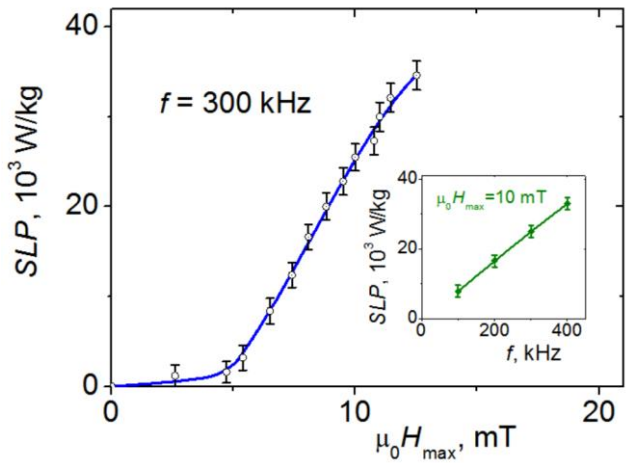


**Fig. 10** *SLP* vs $H_{max}$ dependence measured at $f$ = 300 kHz. Inset shows *SLP* vs $f$ dependence obtained at $\mu_0 H_{max}$ = 10 mT.

It was reported in Refs. [6,7,24,47] that the obtained value is high enough for the use of the MNPs as HT heating mediators in the treatment of cancer diseases. However, the mechanisms responsible for high heating efficiency remain to a large extent unclear.

## 4 Discussion

Magnetic MNPs with a size smaller than a certain critical value $D_{cr}$ are usually in a single domain state, because the energy cost of domain wall formation overweighs any saving in demagnetizing energy.[1,26,37] Theoretical estimations of critical size for strontium-substituted lanthanum manganites $La_{1-x}Sr_xMnO_3$ ($x$ = 0.3) give a $D_{cr}$ value near 70 nm.[26]

The attempts to experimentally determine magnetic single domain critical size in the MNPs of lanthanum-strontium manganites were made in Refs. [42,49]. However, it should be noted that these works were aimed at determination of a *crystallite critical size* ($d_{cr}$), rather than *MNP critical single-domain size* $D_{cr}$. The values of $d_{cr}$ obtained in these works are based on the results of investigation of the dependence of coercivity $H_c$ on a crystallite size $d$, with the values of $d$ being calculated from the broadening of X-ray diffraction peaks. It was found that for the MNPs with $x$ = 0.3, the value of $d_{cr}$ is near 26 nm, while for the MNPs with $x$ = 0.2, $d_{cr} \approx$ 35 nm. Since in our case the average size of LSMO MNPs with $x$ = 0.22 is near 32 nm, a certain part of MNPs could be in vortex or multidomain state, rather than in single domain one.

Below, *the upper limit of SLP* will be estimated for each of the mechanisms of energy losses, described above. The calculations will be carried out under the assumption that the particles are in magnetically single domain state. It was concluded in Ref. [10] that a transition beyond single domain state leads to the narrowing of the hysteresis loop and, correspondingly, to the decrease in *SLP*. This means that the estimations, made below, of the *upper limit of SLP* will also be valid for the case where remagnetization in a certain fraction of MNPs will be incoherent.

### 4.1. Mechanisms of AC losses in LSMO MNPs

Before turning to numerical calculations, let us note two characteristic features of the experimental data on heating efficiency of LSMO MNPs. First, the dependence of *SLP* on AMF amplitude is of threshold character: *SLP* becomes noticeable only when $H_{max}$ exceeds a certain value (see Fig. 10). Second, the *SLP* is almost linear function of AMF frequency (see inset of Fig. 10). Such kind of *SLP*($H_{max}$) and *SLP*($f$) dependences is characteristic only for SW-losses. As follows from formulae (2.2) – (2.9), EC-, NR- and BR-losses display quadratic dependence on AMF amplitude. What concerns frequency dependence of *SLP*, EC-, NR- and BR-losses either display quadratic *SLP*($f$) dependence, or are frequency independent.

Thus, the character of *SLP*($H_{max}$) and *SLP*($f$) dependences points to the fact that the mechanism which is responsible for LSMO MNP heating is SW-mechanism. One should expect that, even if there are contributions from other mechanisms, they will be of less importance.

Let us estimate energy losses caused by each of the mechanisms discussed in Section 2. Make calculations for such MNP parameters: $\sigma = 10^6\ \Omega^{-1}\text{m}^{-1}$, $M_s^m$ = 50 A·m$^2$/kg (at room temperature), $R$ = 16 nm. The volume of MNP is $1.7\cdot10^{-23}$ m$^3$. Assume that the MNP density is the same as that of bulk LSMO:[50] $\rho^{LSMO}$ = 6400 kg/m$^3$. Then $M_s = M_s^m \cdot \rho^{LSMO}$ = 320 kA/m. Consider a case where magnetic fluid is a mixture of LSMO MNPs and water ($\eta \approx 10^{-3}$ Pa·s) and 1 mL of the fluid contains 50 mg of MNPs ($m^{MNP}$ = 50 kg/m$^3$, where $m^{MNP}$ is the total MNP mass in 1 m$^3$ of magnetic fluid). Make estimations of losses when magnetic fluid is subjected to the action of AMF with parameters: $f$ = 300 kHz, $\mu_0 H_{max}$ = 10 mT.

**4.1(A). EC-losses.** $P_{EC}$ can be calculated using formula (2.2):

$$P_{EC} = \frac{\sigma}{5}\pi^2 f^2 \mu_0^2 (H_{max} + M_{max})^2 R^2 \approx 1.4\ \text{W/m}^3 \qquad (4.1)$$

$$SLP_{EC} = P_{EC} / \rho^{LSMO} \approx 0.2\cdot10^{-3}\ \text{W/kg} \qquad (4.2)$$

Here, $M_{max}$ was estimated from $M(H)$ dependence at 295 K: $M_{max} \equiv M(\mu_0 H_{max}$ = 10 mT) ≈ 130 kA/m.

Thus, *SLP* resulted from EC-losses is by 7 orders of magnitude smaller than experimentally obtained value.

**4.1(B1). NR-losses.** Since the value of low-frequency blocking temperature, $T_b^{lf}$, is slightly lower than room temperature, the value of $T_b^{hf}$ is expected to exceed room temperature (see considerations in Section 2.2). This makes it unlikely that NR-losses are realized in MNPs under study. What is more, the character of experimental *SLP*($H_{max}$) and *SLP*($f$) dependences does not agree with theoretical calculations for NB mechanism.

**4.1(B2). SW-losses.** It was noted above that for MNPs with random orientations of easy axes the upper limit of $P_{SW}$ is determined by formula (2.13):

$$P_{SW}^{limit} = 4\cdot\alpha\cdot\mu_0 H_{max} M_s f\big|_{\alpha=0.39} \approx 1.5\cdot10^9\ \text{W/m}^3. \qquad (4.3)$$

$$SLP_{SW}^{limit} = P_{SW} / \rho^{LSMO} = 234\cdot10^3\ \text{W/kg}. \qquad (4.4)$$

Typical values of $\alpha$ which have been observed in experiments are in the range from 0.01 to 0.3.[10,31] This means that in our case one can expect $SLP_{SW}$ from $6\cdot10^3$ to $180\cdot10^3$ W/kg.

**4.1(C). BR-losses.** As follows from formula (2.14), the Brown relaxation time $\tau_B$ depends on hydrodynamically effective radius of a nanoparticle. In a majority of cases for the MNPs relevant to magnetic HT, $R_h$ exceeds geometrical radius $R$ by a few nanometers.[4,7,51,52] Keeping in mind the remarks made in Subsection 2.2(C), let us estimate the upper limit for BR-losses, assuming that $R_h = 1.5R$ and the MNPs are monodisperse:

$$\tau_B = \frac{4\pi\eta R_h^3}{k_B T} \approx 4.2\cdot10^{-5}\ \text{s}. \qquad (4.5)$$

$$P_{BR}^{mono} = \frac{2\mu_0\pi^2 f^2 \tau_B}{1+(2\pi f\tau_B)^2}\chi_0 H_{max}^2 \approx 1.4\cdot10^7\ \text{W/m}^3, \qquad (4.6)$$

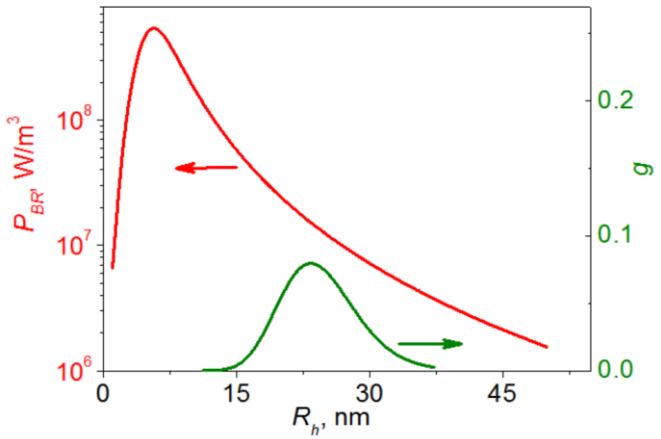


Fig. 11. The BR power losses $P_{BR}$ (red solid line) as a function of hydrodynamic radius $R_h$, calculated for LSMO MNPs under study. Green solid line shows the probability density function $g(R_h)$ for the same MNPs.

$$SLP_{BR}^{mono} = P_{BR} / \rho^{\mathrm{LSMO}} = 2.2 \cdot 10^3 \ \mathrm{W/kg}. \qquad (4.7)$$

It follows from formulae (4.5) – (4.6) that small variations in $R_h$, in particular due to polydispersity, may cause strong changes in $P_{BR}$. The account for the particles pylydispersity will give more precise estimations of $P_{BR}$.

Red solid line in Fig. 11 presents the dependence of the BR power losses $P_{BR}$ on hydrodynamic radius $R_h$, calculated for LSMO MNPs under study. As follows from the numerical analysis of the microphotographs of LSMO MNPs, the particle sizes are log-normally[53] distributed (see solid line in Fig. 6(b)). Assuming that the hydrodynamic radii of MNPs obey the same distribution, the value of $P_{BR}$ can be calculated as

$$P_{BR}^{poly} = \int_{R_{h\min}}^{R_{h\max}} P_{BR}(R_h) V(R_h) g(R_h) dR_h \Big/ \int_{R_{h\min}}^{R_{h\max}} V(R_h) g(R_h) dR_h \approx$$

$$\approx 2.3 \cdot 10^6 \ \mathrm{W/m^3}, \qquad (4.8)$$

which gives

$$SLP_{BR}^{poly} = P_{BR} / \rho^{\mathrm{LSMO}} \approx 0.4 \cdot 10^3 \ \mathrm{W/kg}. \qquad (4.9)$$

Here, $V(R_h)$ is the volume of MNPs with a radius $R_h$, $g(R_h)$ is the probability density function (see Fig. 11, green solid line), $R_{hj}$ = $1.5 \cdot R_j$, where $R_j$ = 5 and 50 nm for $j$ = min and max, respectively (see Fig. 6). The analysis of expression (4.8) shows that the narrower size distribution is, the higher is the $P_{BR}$ value.

It is evident that the calculated $SLP_{BR}$ value is by far smaller than experimentally obtained $SLP$ at $\mu_0 H_{\max}$ = 10 mT (see Fig. 10). At the same time, one cannot exclude that BR mechanism may play important role at weak magnetic fields ($\mu_0 H_{\max}$ < 5 mT), where SW-losses are negligible.

As a result, it follows from the calculations that only SW-mechanism can provide sufficiently high energy losses which correspond to experimentally obtained value $SLP(\mu_0 H_{\max}$ = 10 mT) ≈ $25 \cdot 10^3$ W/kg; the other kinds of AC losses are so weak that they cannot be responsible for LSMO MNPs heating. It also follows from the calculations that $SLP$ can be increased by about an order of magnitude by means of optimization of the parameters of LSMO MNPs (weakening agglomeration, narrowing size distribution, attaining uniformity of geometrical and magnetic parameters) and corresponding adjustment of AMF parameters.

## 5 Conclusions

In this work, the mechanisms of AC losses in an ensemble of MNPs subjected to the action of AMF are described, and domains of their validity are analyzed. It is stressed that the approach to model remagnetization processes and calculate SLP values at high frequencies (~100 kHz) with the use of MNP magnetic parameters extracted from magnetostatic measurements is not always correct. Due to the fact that blocking temperature and coercivity are frequency dependent, remagnetization processes at high frequencies may be qualitatively different from those at low frequencies.

Experiments on the nanoparticles of $La_{1-x}Sr_xMnO_3$ ($x$ = 0.22) manganites and magnetic fluids based on them have been carried out. Energy losses originated from different mechanisms of AC losses have been analyzed and calculated. Based on the character of $SLP(H_{\max})$ and $SLP(f)$ dependences, as well as on the results of calculations, it is reliably established that only SW-mechanism can provide sufficiently high losses which are comparative to experimentally obtained value; the other kinds of AC losses are so weak that they cannot be responsible for LSMO MNPs heating.

It should be noted that the conclusion about leading role of SW-mechanism is somewhat unexpected, since one would expect rather small values of coercivity and magnetization in the vicinity of LSMO Curie point (~320 K). Although this topic needs further investigations, the results obtained clearly demonstrate the prospectivity of the use of the nanoparticles of $La_{1-x}Sr_xMnO_3$ manganites as self-controlled heating mediators in magnetic HT.

## Acknowledgements

The work is partly supported by the Programs on Fundamental Studies of the National Academy of Sciences of Ukraine (1.4 VC/157 and “FineChemicals”)

## Notes and references

1 *Nanomagnetism: Fundamentals and Applications*, Ed. by Chris Binns, Elsevier, 2014, ISBN: 978-0-08-098353-0, 328 p.
2 S.D. Bader, *Rev. Mod. Phys*., 2006, 78, 1.
3 Q.A. Pankhurst, J. Connolly, S.K. Jones and J. Dobson. *J. Phys. D: Appl. Phys.*, 2003, 36, R167.
4 R. Hergt, S. Dutz, R. Müller and M. Zeisberger, *J. Phys.: Cond. Matter*., 2006, **18**, S2919.
5 A. Jordan, R. Scholz, P. Wust, H. Fähling and R. Felix, *J. Magn. Magn. Mater*., 1999, **201**, 413.
6 A. Belous, S. Solopan, A. Yelenich, L. Bubnovskaya and S. Osinsky, *Proc. IEEE XXXIII International Scientific Conference Electronics and Nanotechnology (ELNANO-2013)*, 2013, 280.
7 R.E. Rosensweig, *J. Magn. Magn. Mater*., 2002, **252**, 370.

8 A.G. Belous, S.O. Solopan, O.V. Yelenich, A.I. Tovstolytkin, T.V. Kolodiazhnyi, S.P. Osinsky and L.N. Bubnovskaya, AIP Conf. Proc., 2014, **1627**, 13.
9 W.J. Atkinson, I.A. Brezovich and D.P. Chakraborty, *IEEE Trans. Biomed. Eng*., 1984, **31**, 70.
10 B. Mehdaoui, A. Meffre, J. Carrey, S. Lachaize, L.-M. Lacroix, M. Gougeon, B. Chaudret and M. Respaud, *Adv. Func. Mater*., 2011, **21**, 4573.
11 P. de la Presa, Y. Luengo, M. Multigner, R. Costo, M.P. Morales, G. Rivero and A. Hernando, *J. Phys. Chem. C*., 2012, **116**, 25602.
12 R. Chen, M.G. Christiansen and P. Anikeeva, *ACS Nano*, 2013, **7**, 8990.
13 S. Dutz and R. Hergt, *Nanotechnology*, 2014, **25**, 452001.
14 A. Ito, K. Tanaka, K. Kondo, M. Shinkai, H. Honda, K. Matsumoto, T. Saida, and T. Kobayashi, *Cancer Sci*., 2003, **94**, 308.
15 S. Mornet. S. Vasseur, F. Grasset and E. Duguet, *J. Mater. Chem*., 2004, **14**, 2161.
16 P. Moroz, S.K. Jones and B.N. Gray, *Int. J. Hyperthermia*, 2002, **18**, 267.
17 A. Jordan, R. Scholz, K. Maier-Hau, M. Johannsen, P. Wust, J. Nadobny, H. Schirra, H. Schmidt, S. Deger, S. Loening, W. Lanksch and R. Felix, *J. Magn. Magn. Mater*., 2001, **225**, 118.
18 F. Grasset, S. Mornet, A. Demourgues, J. Portier, J. Bonnet, A. Vekris and E. Duguet, *J. Magn. Magn. Mater*., 2001, **234**, 409.
19 S. Vasseura, E. Dugueta, J. Portiera, G. Goglioa, S. Morneta, E. Hadova , K. Knızek, M. Marysko, P. Veverka and E. Pollert. *J. Magn. Magn. Mater*., 2006, **302**, 315.
20 N.K. Prasad, K. Rathinasamy, D. Panda and D. Bahadur, *J. Biomed. Mater. Res. Part B: Appl. Biomater*., 2008, **85B**, 409.
21 M. Veverka, K. Zaveta, O. Kaman, P. Veverka, K. Knizek, E. Pollert, M. Burian and P. Kaspar, *J. Phys. D: Appl. Phys*., 2014, **47**, 065503.
22 C.L. Ondeck, A.H. Habib, P. Ohodnicki, K. Miller, C.A. Sawyer, P. Chaudhary and M.E. McHenry, J. Appl. Phys., 2009, **105**, 07B324.
23 A.A. Kuznetsov, O.A. Shlyakhtin, N.A. Brusentsov and O.A. Kuznetsov, *Europ. Cells and Mater*., 2002, **3**, 75.
24 E. Pollert, O. Kaman, P. Veverka, M. Veverka, M. Marysko, K. Zaveta, M. Kacenka, I. Lukes, P. Jendelova, P. Kaspar, M. Burian and V. Herynek, *Phil. Trans. Roy. Soc. A*, 2010, **368**, 4389.
25 A. Rashid, A. Ahmed, S.N. Ahmad, S.A. Shaheen and S**.** Manzoor. *J. Magn. Magn. Mater*., 2013, **347**, 39.
26 D.H. Manh, P.T. Phong, P.H. Nam, D.K. Tung, N.X. Phuc and In-Ja Lee, *Physica B*, 2014, **444**, 94.
27 A. Urushibara, Y. Moritomo, T. Arima, A. Asamitsu, G. Kido and Y. Tokura, *Phys. Rev. B*, 1995, **51**, 14103.
28 A.G. Belous, O.I. V'yunov, E.V. Pashkova, O.Z. Yanchevskii, A.I. Tovstolytkin and A.M. Pogorelyi, *Inorg. Mater*., 2003, **39**, 161.
29 V.M. Kalita, A.F. Lozenko, S.M. Ryabchenko, A.A. Timopheeev, R.A. Trotsenko, I.A. Danilenko and T.E. Konstantinova, *Low Temp. Phys*., 2008, **34**, 436.
30 O.V. Yelenich, S.O. Solopan, T.V. Kolodiazhnyi, V.V. Dzyublyuk, A.I. Tovstolytkin and A.G. Belous, *Solid State Sciences*, 2013, **20**, 115.
31 J. Carrey, B. Mehdaoui and M. Respaud, *J. Appl. Phys*., 2011, **109**, 083921.
32 S. Ruta, R. Chantrell and O. Hovorka, *arXiv: 1412.3814v1*, 2014.
33 G. Vallejo-Fernandez, O. Whear, A.G. Roca, S. Hussain, J. Timmis, V. Patel and K.O'Grady, *J. Phys. D: Appl. Phys*., 2013, **46**, 312001.
34 D.L. Lyfar, S.M. Ryabchenko, V.N. Krivoruchko, S.I. Khartsev and A.M. Grishin, *Phys. Rev. B*, 2004, **69**, 100409(R).
35 A.K. Pradhan, R. Bah, R.B. Konda, R. Mundle, H. Mustafa, O. Bamiduro and R.R. Rakhimov, *J. Appl. Phys*., 2008, **103**, 07F704.
36 R. Porwal, R.P. Pant and R.C. Budhani, *J. Appl. Phys*., 2015, **117**, 013904.
37 S. Bedanta and W. Kleemann. *J. Phys. D: Appl. Phys*., 2009, **42**, 013001.
38 S. Chikazumi, *Physics of Ferromagnetism*. Oxford University Press, New York, 2005.
39 A.I. Nandapure, S.B. Kondawar, P.S. Sawadh and B.I. Nandapure, *Physica B*, 2012, **407**, 1104.
40 D.X. Chen, V. Skumryev and H. Kronmuller, *Phys. Rev. B*, 1992, **46**, 3496.
41 O.V. Yelenich, S.O. Solopan, T.V. Kolodiazhnyi, V.V. Dzyublyuk, A.I. Tovstolytkin and A.G. Belous, *Mater. Chem. Phys.*, 2014, **146**, 129.
42 S. Daengsakul, C. Thomas, C. Mongkolkachit and S. Maensiri, Solid State Sciences, 2012, **14**, 1306.
43 S.O. So
44 lopan, O.I. V'yunov, A.G. Belous, T.I. Polek and A.I. Tovstolytkin, *Solid State Sciences*, 2012, **14**, 501.
45 B.L. Cushing, V.L. Kolesnichenko and C.J. O'Connor, *Chem. Rev*., 2004, **104**, 3893.
46 V. Pillai, P. Kumar, M.S. Multani and D.O. Shah, *Colloids and Surfaces A: Physicochemical and Engineering Aspects*, 1993, **80**, 69.
47 T. Kida, G. Guan, Y. Minami, T. Ma and A. Yoshida, *J. Mater. Chem*., 2003, **13**, 1186.
48 S. Solopan, A. Belous, A. Yelenich, L. Bubnovskaya, A. Kovelskaya, A. Podoltsev, I. Kondratenko and S. Osinsky, *Experimental Oncology*, 2011, **33**, 130.
49 D. Peddis, F. Orrù, A. Ardu, C. Cannas, A. Musinu and G. Piccaluga, *Chem. Mater*., 2012, **24**, 1062.
50 P. Dey and T.K. Nath, *Appl. Phys. Lett*., 2006, **89**, 163102.
51 X. Moya, L.E. Hueso, F. Maccherozzi, A.I. Tovstolytkin, D.I. Podyalovskii, C. Ducati, L. Phillips, M. Ghidini, O. Hovorka, A. Berger, M.E. Vickers, E. Defaÿ, S.S. Dhesi and N.D. Mathur, *Nature Mater*., 2013, **12**, 52.
52 M. Ma, Y. Wu, J. Zhou, Y. Sun, Y. Zhang and N. Gu. *J. Magn. Magn. Mater*., 2004, **268**, 33.
53 E. Lima Jr., T.E. Torres, L.M. Rossi, H.R. Rechenberg, T.S. Berquo, A. Ibarra, C. Marquina, M.R. Ibarra and G.F. Goya, *J. Nanopart. Res*., 2013, **15**, 1654.
54 E. Babinsky, P.E. Sojka, *Progr. Energy Comb. Sci*., 2002, **28**, 303.